

Supporting Information

Chiral Polymorphism in the Self-Assemblies of an Achiral Molecule Induced by the Multiple Hydrogen Bonds

Kai Miao, Yi Hu, Li Xu, Meiqiu Dong, Juntian Wu, Xinrui Miao*, Wenli Deng*

College of Materials Science and Engineering, South China University of Technology, Wushan Road,

Tianhe District, Guangzhou 510640, P.R. China.

E-mail: msxrmiao@scut.edu.cn; wldeng@scut.edu.cn; Tel: (+86)020-2223670

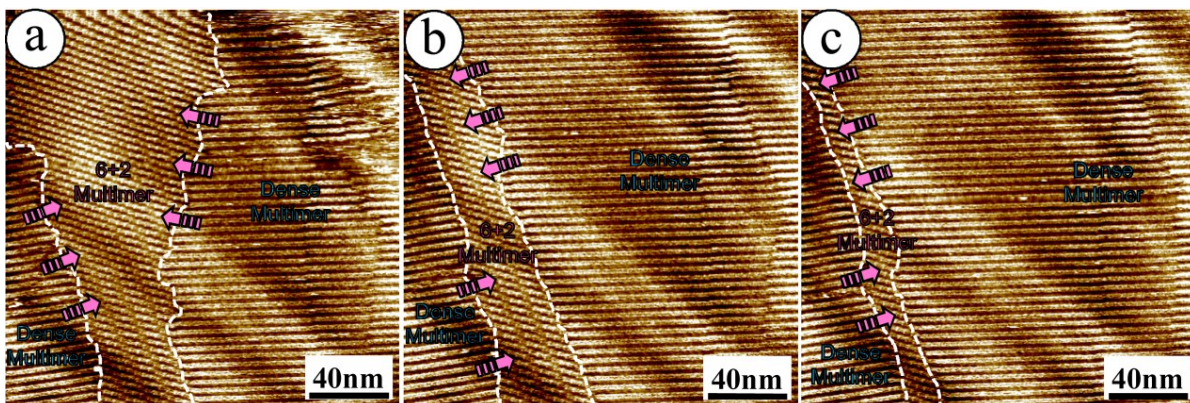


Fig. S1 Phase transition from “6-2” multimer to densely-packed pattern of HPF molecules at the pure 1-octanol/HOPG interface. Image conditions: $I_{\text{set}} = 571 \text{ pA}$, $V_{\text{bias}} = 659 \text{ mV}$. $C_{\text{HPF}} = 3.0 \times 10^{-5} \text{ mol L}^{-1}$.

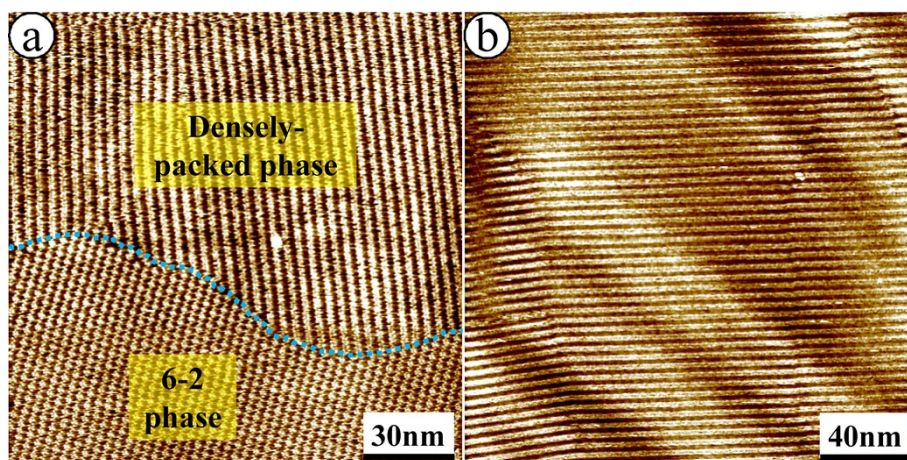


Fig. S2 (a) Large-scale STM image of the coexisted densely-packed and “6-2” patterns of HPF molecule on the HOPG surface. (b) Large-scale STM image of the densely-packed pattern after being heating at $50 \text{ }^\circ\text{C}$. Image conditions are $I_{\text{set}} = 513\text{--}527 \text{ pA}$ and $V_{\text{bias}} = 670\text{--}685 \text{ mV}$.

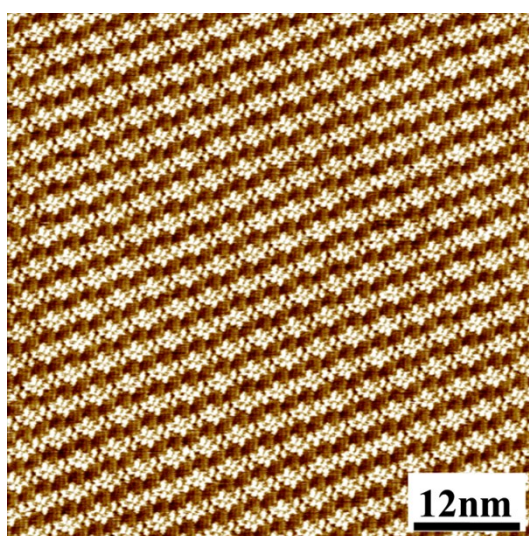


Fig. S3 Large-scale STM image of chiral “6-2” multimer of HPF molecules at the pure 1-octanol/HOPG interface. Image conditions: $I_{\text{set}} = 573 \text{ pA}$, $V_{\text{bias}} = 677 \text{ mV}$. $C_{\text{HPF}} = 3.0 \times 10^{-5} \text{ mol L}^{-1}$.

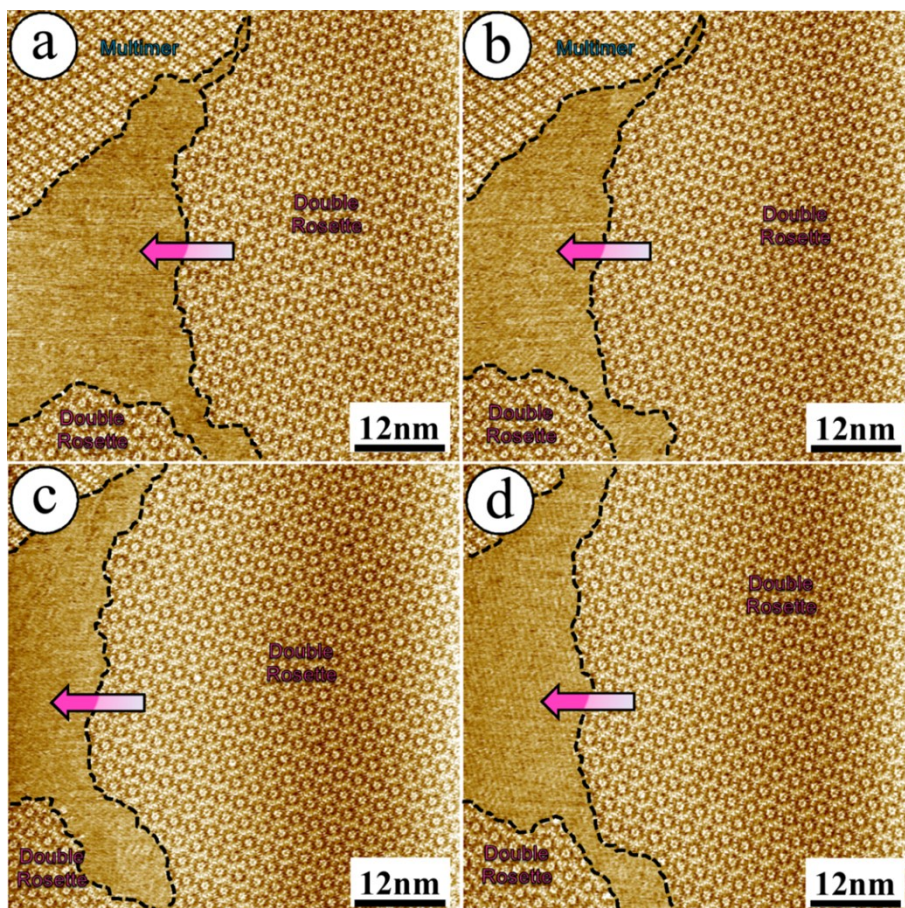


Fig. S4 (a) Sequential STM images showing the coexisted double rosette pattern and alternate pattern of HPF molecules in mixed solvents (1-octanoic acid/1-octanol = 8/1, v/v) on the HOPG surface. No obvious phase transition was observed during the scanning process. Concentration = $3.0 \times 10^{-5} \text{ mol L}^{-1}$. Scanning conditions: $I_{\text{set}} = 577 \text{ pA}$, $V_{\text{bias}} = 660 \text{ mV}$.

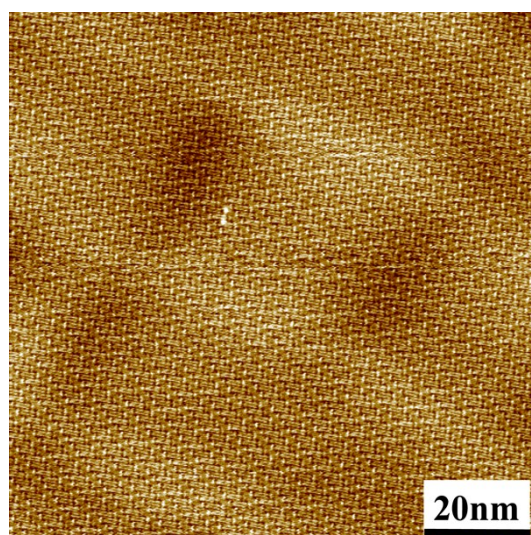


Fig. S5 Large-scale STM image of the zigzag pattern of the system after being heating at 50 °C. Image conditions are $I_{\text{set}} = 525 \text{ pA}$ and $V_{\text{bias}} = 673 \text{ mV}$.

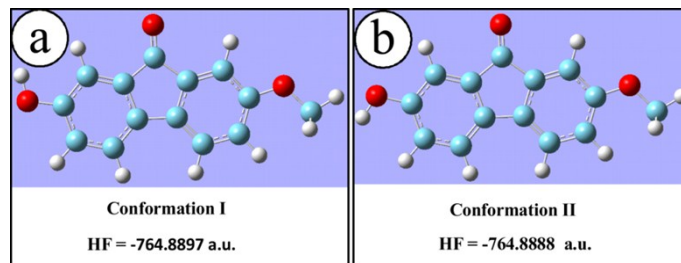


Fig. S6 Calculations for HPF molecule with different conformations, wherein the hydroxyl group is characterized with (a) upward orientation (termed as “*cis*-conformer”) and (b) downward orientation (termed as “*trans*-conformer”).

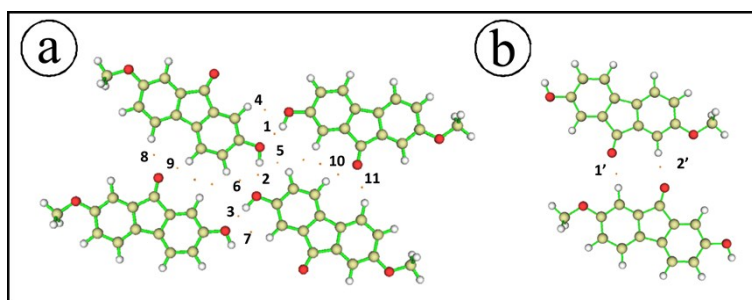


Fig. S7 (a, b) Topology analysis of the windmill-like tetramer and dimer units showing the presence of intermolecular hydrogen bonds.

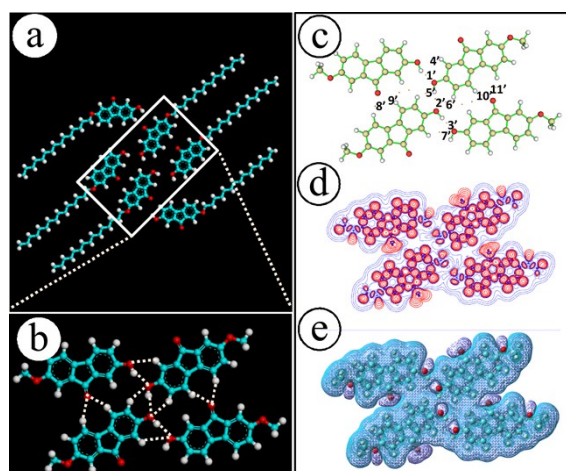


Fig. S8 (a) Structural model shows the unit I (hexamer) of the CW “6-2” pattern in the HPF monolayer. (b) Close inspection of the optimized tetramer (windmill node) within each hexamer, wherein the intermolecular hydrogen bonds are depicted by the white dashed lines. (c) Topology analysis of the windmill showing the formation of intermolecular hydrogen bonds. (d–e) 2D and 3D charge deformation density maps allow for an intuitive observation of the intermolecular hydrogen bonds within the windmill node.

Table S1. Structural parameters, topological properties of the electron density at the critical points relative to the intermolecular hydrogen bonds for the CW tetramer.

Type of Intermolecular Hydrogen Bonds	Sequential Number	Bond Length (Å)	Bond Angle (°)	ρ_{CP} ($e \text{ \AA}^{-3}$)	$\nabla^2\rho_{CP}$ ($e \text{ \AA}^{-5}$)	G_{CP} ($\text{kJ mol}^{-1} \text{ bohr}^{-3}$)	V_{CP} ($\text{kJ mol}^{-1} \text{ bohr}^{-3}$)	H_{CP} ($\text{kJ mol}^{-1} \text{ bohr}^{-3}$)
-OH...O(hydroxyl)-	1'	1.95	154.77	0.1621	2.0122	55.94	-57.06	-1.13
	2'	2.12	175.91	0.1102	1.3433	37.01	-37.44	-0.43
	3'	1.96	179.65	0.1543	1.9219	53.11	-53.87	-0.76
	4'	2.61	130.07	0.04142	0.6109	13.76	-10.89	2.88
-C(sp ²)-H...O(hydroxyl)-	5'	2.42	144.42	0.07493	1.2104	27.74	-22.51	5.23
	6'	2.44	142.96	0.06671	0.8730	21.37	-18.96	2.41
	7'	2.82	126.11	0.03058	0.4370	9.510	-7.11	2.39
	8'	2.46	157.54	0.05587	0.7768	18.40	-15.65	2.75
	9'	2.23	158.02	0.1019	1.2298	32.48	-31.47	1.01
	10'	2.21	161.41	0.1063	1.2993	34.29	-33.19	1.10
	11'	2.50	156.89	0.05077	0.7113	16.62	-13.87	2.75

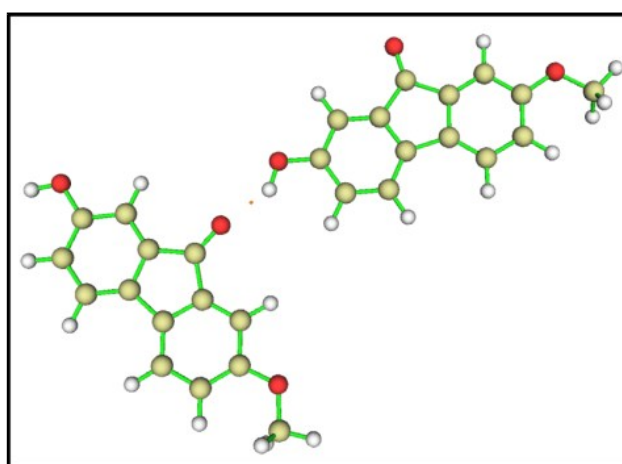


Fig. S9 Topology analysis of the dimer unit for the inner rosette showing the presence of intermolecular hydrogen bonds.

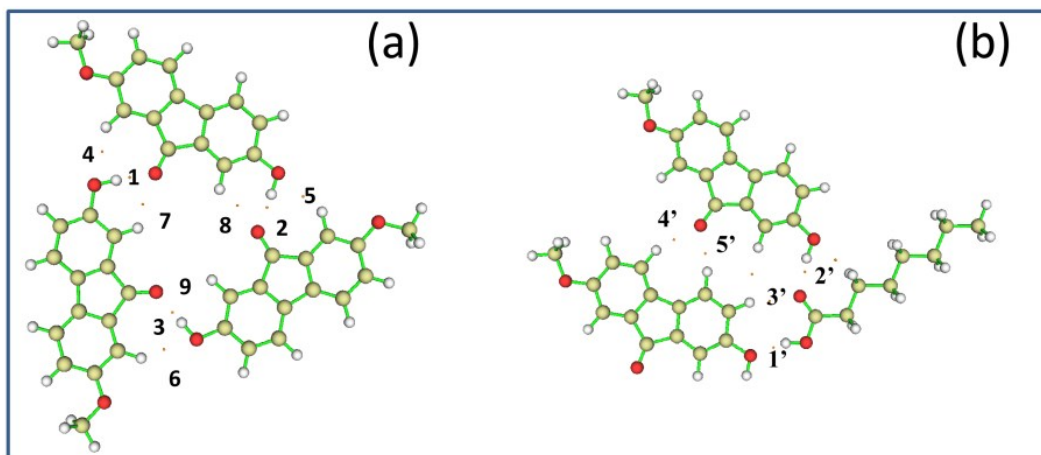


Fig. S10 (a, b) Topology analysis of the trimer and dimer units for the outer rosette pattern showing the presence of intermolecular hydrogen bonds.

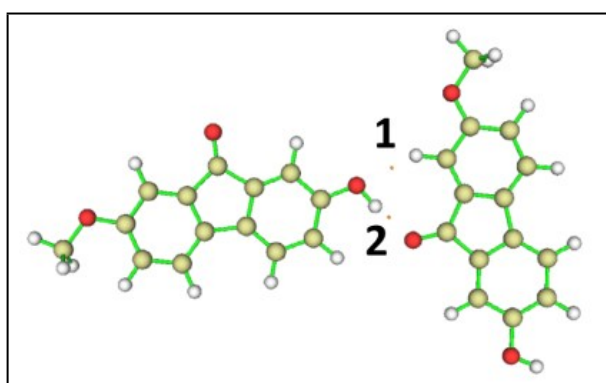


Fig. S11 Topology analysis of the dimer unit for the zigzag pattern showing the presence of intermolecular hydrogen bonds.

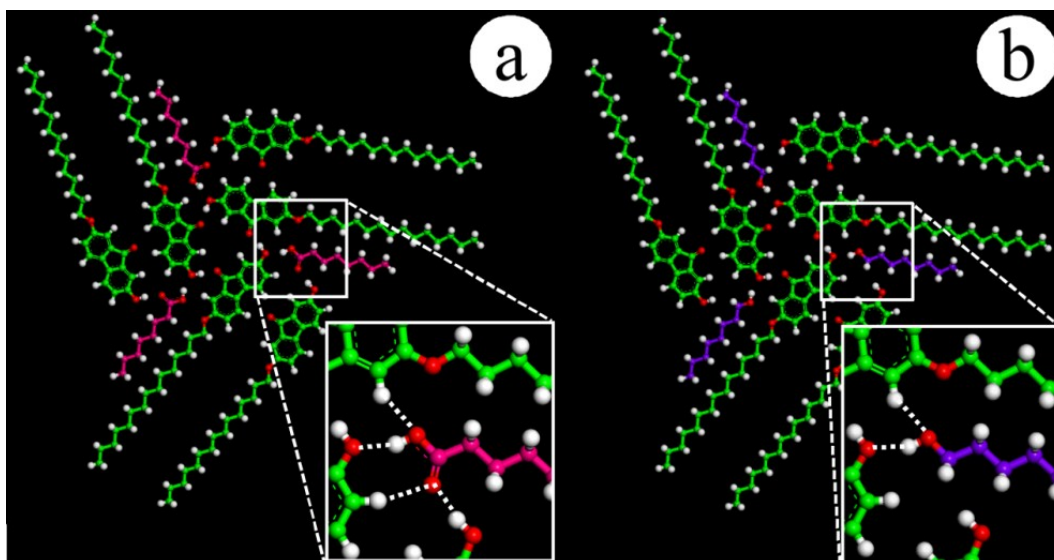


Fig. S12 Proposed structural models illustrating the differences in the stability of the outer hexamer arising from the co-adsorbed (a) 1-octanoic acid and (b) 1-octanol.

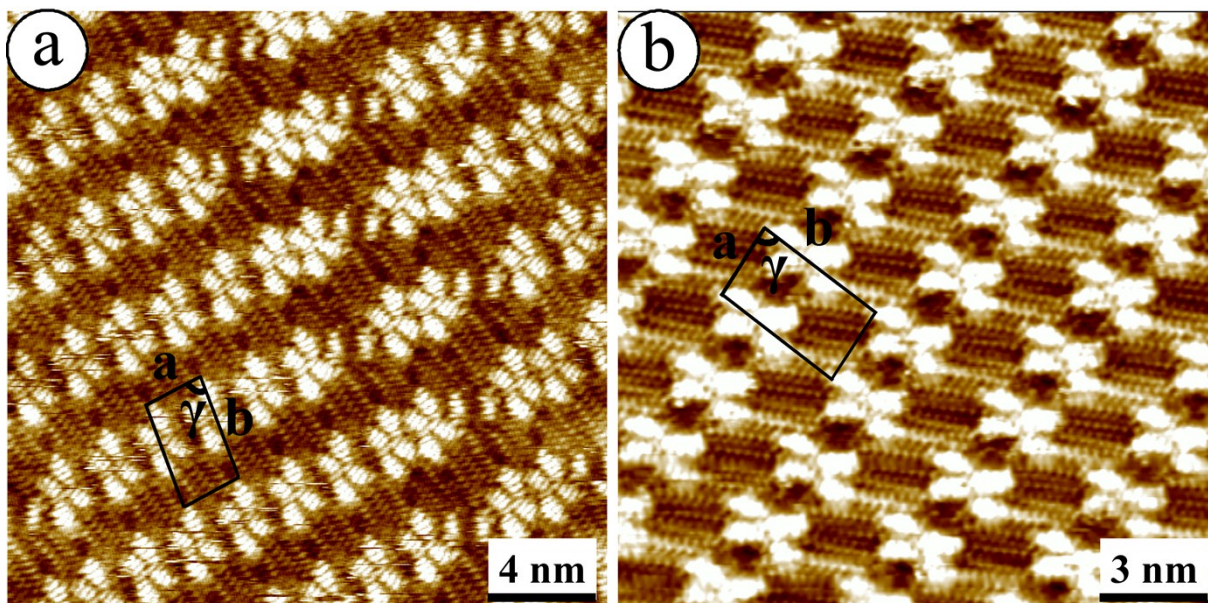


Fig. S13 (a) HR-STM image of chiral tetramer of HPF molecules in mixed solvents (1-octanoic acid/1-octanol = 8/1, v/v) on the HOPG surface. Concentration: $3.0 \times 10^{-5} \text{ mol L}^{-1}$. Scanning conditions: $I_{\text{set}} = 663 \text{ pA}$, $V_{\text{bias}} = 577 \text{ mV}$. (b) HR-STM image of chiral tetramer of HPF molecules in pure 1-octanoic acid on the HOPG surface. Concentration: $3.0 \times 10^{-5} \text{ mol L}^{-1}$. Scanning conditions: $I_{\text{set}} = 655 \text{ pA}$, $V_{\text{bias}} = 578 \text{ mV}$.

The tetramer in the alternate monolayer is featured with unit parameters of $a = 1.9 \pm 0.2 \text{ nm}$, $b = 3.5 \pm 0.2 \text{ nm}$ and $\gamma = 79.0 \pm 1.0^\circ$. Each unit is composed of four HPF molecules and the molecular packing density is 0.61 nm^{-2} per molecule. While at the pure 1-octanoic acid/HOPG interface, the tetramer possesses almost the identical structural characteristics, with the unit cell parameters of $a = 2.0 \pm 0.1 \text{ nm}$, $b = 3.4 \pm 0.1 \text{ nm}$ and $\gamma = 79.0 \pm 1.0^\circ$, giving rise to the close molecular packing density (0.60 nm^{-2} per molecule). Given the fact that the proximity in the unit cell parameters as well as the packing densities for the tetramer pattern both in mixed solvents and 1-octanoic acid within the experimental errors, it is reasonable to speculate those two structures belong to the same pattern.

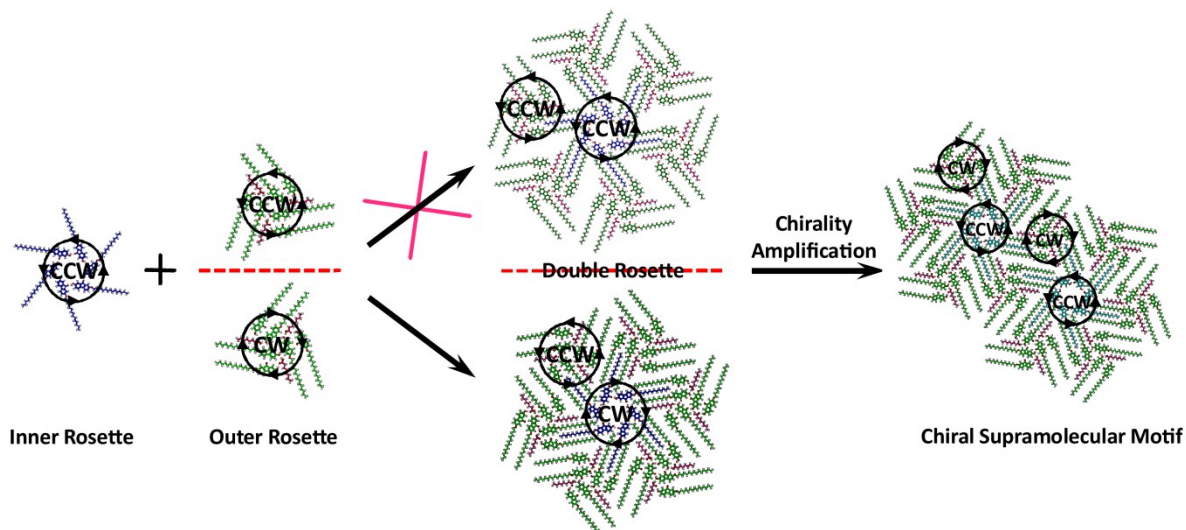


Fig. S14 Possible scheme showing the induction and amplification process of CCW double-rosette monolayer.

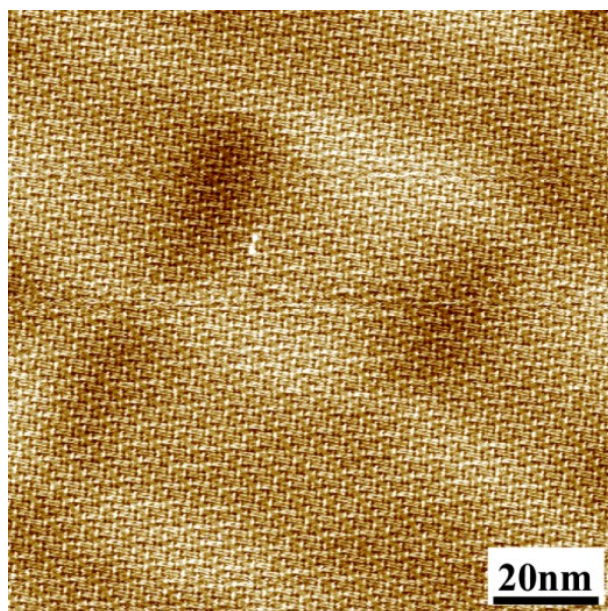


Fig. S15 Large-scale STM image shows the zigzag pattern in the HPF monolayer at the solid-gas interface. Image conditions: $I_{\text{set}} = 677 \text{ pA}$, $V_{\text{bias}} = 579 \text{ mV}$. $C_{\text{HPF}} = 3.0 \times 10^{-5} \text{ mol L}^{-1}$.

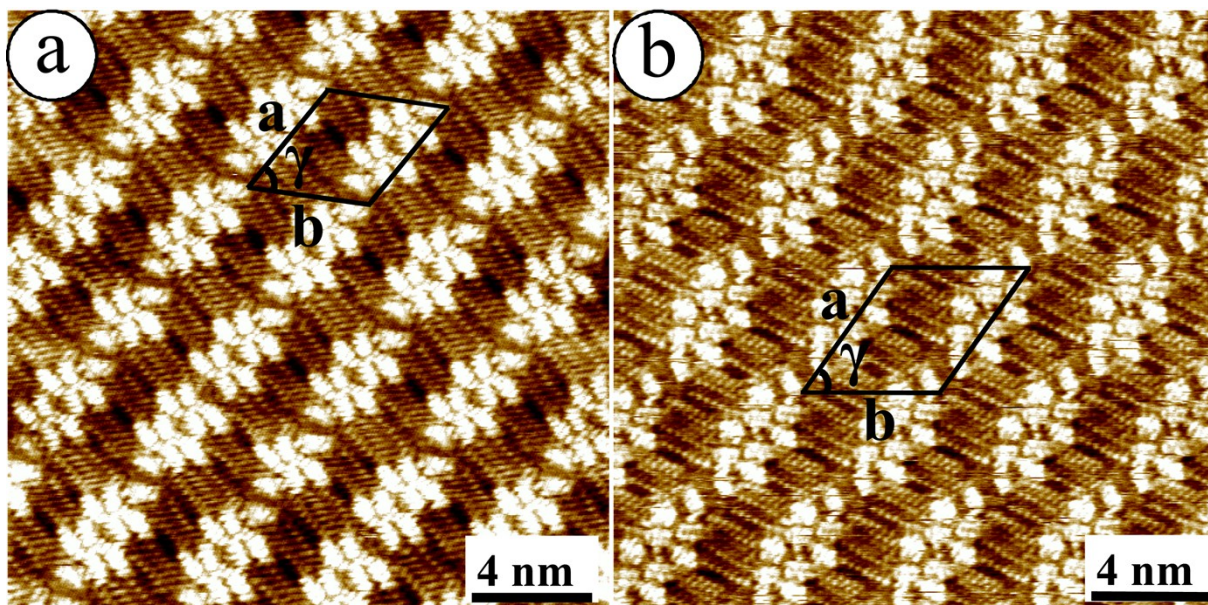


Fig. S16 HR-STM image of chiral decamer of HPF molecules in mixed solvents (1-octanoic acid/1-octanol = 5/1, v/v) on the HOPG surface. (a) Image conditions: $I_{\text{set}} = 563$ pA, $V_{\text{bias}} = 652$ mV. $C_{\text{HPF}} = 3.0 \times 10^{-5}$ mol L^{-1} . (b) Image conditions: $I_{\text{set}} = 557$ pA, $V_{\text{bias}} = 655$ mV. $C_{\text{HPF}} = 3.0 \times 10^{-5}$ mol L^{-1} .